Ultrastructural Morphology of the Optic Nerve Head in Aged and Glaucomatous Mice

Ying Zhu,[1,2] Anthony C. Pappas,[2] Rui Wang,[2,3] Philip Seifert,[2] Daniel Sun,[2] and Tatjana C. Jakobs[2]

[1]Department of Ophthalmology, Tongji Hospital, Huazhong University of Science and Technology, Wuhan, Hubei, China
[2]Department of Ophthalmology, Massachusetts Eye and Ear Infirmary/Schepens Eye Research Institute, Harvard Medical School, Boston Massachusetts, United States
[3]Department of Ophthalmology, The First Hospital of Xi'an, Xi'an, Shaanxi, China

Correspondence: Tatjana C. Jakobs, Schepens Eye Research Institute, 20 Staniford Street, Boston, MA 02114, USA;
Tatjana_Jakobs@meei.harvard.edu.

Submitted: January 16, 2018
Accepted: July 13, 2018

Citation: Zhu Y, Pappas AC, Wang R, Seifert P, Sun D, Jakobs TC. Ultrastructural morphology of the optic nerve head in aged and glaucomatous mice. *Invest Ophthalmol Vis Sci*. 2018;59:3984–3996. https://doi.org/10.1167/iovs.18-23885

Purpose. To study age- and intraocular pressure–induced changes in the glial lamina of the murine optic nerve on the ultrastructural level.

Methods. Naïve C57bl/6 mice at various ages spanning the time between early adulthood (3 months) and senescence (30 months) were used in this study. In addition, the intraocular pressure (IOP) was increased in a group of young mice by injection of microbeads into the anterior chamber. The unmyelinated segments of the optic nerve containing the glial lamina were prepared for transmission electron microscopy and imaged at high resolution.

Results. Axon packing density decreased slightly with age. Aging nerves contained higher numbers of enlarged and degenerating axons. Mean axonal diameter and in particular the variance of axonal diameter correlated well with age. Axonal mitochondria also showed age-dependent signs of pathology. The mean diameter of axonal mitochondria increased, and aged axons often contained profiles of mitochondria with very few or no cristae. Astrocytic mitochondria remained normal even in very old nerves. Changes to axons and axonal mitochondria in young glaucomatous nerves were comparable with those of 18- to 30-month-old naïve mice. In addition to axons and mitochondria, aged and glaucomatous nerves showed thickening of the blood vessel basement membranes and increased deposition of basement membrane collagen.

Conclusions. On the ultrastructural level, the effects of age and elevated IOP are quite similar. One month of elevated IOP seems to have as strongly detrimental effects on the nerve as at least 18 months of normal aging.

Keywords: aging, glaucoma, optic nerve head, electron microscopy

Glaucoma is a common cause of vision loss and blindness that is characterized by an optic neuropathy and the progressive degeneration of retinal ganglion cells.[1,2] Among the risk factors for the disease are elevated IOP, genetic factors, and age.[3–7] All current glaucoma therapies aim at lowering the IOP by pharmacologic or surgical means. In addition, neuroprotective approaches and gene therapies are in the experimental stage and several show promise, at least in animal models.[8–10] However, age itself is a risk factor that cannot be modified. It has been hypothesized that aging causes multiple detrimental effects on the eye and the optic nerve, each of which may not reach a clinical threshold but make the eye more susceptible to glaucomatous neurodegeneration. Such aging effects may, for example, be metabolic,[11] mitochondrial,[12–14] immunologic, or vascular,[15] or involve connective tissue stiffening in the anterior chamber, the sclera, or the lamina cribrosa.[16–19] In the present study, we focused on aging effects on the optic nerve, in particular on the unmyelinated segment, because experimental evidence points to this region as the locus of initial insult to retinal ganglion cell axons in glaucoma.[20–22]

The optic nerve consists almost entirely of the fibers of the retinal ganglion cells in transit from the eye to the lateral geniculate body and the superior colliculus. In the first segment, directly behind the globe, the fibers are unmyelinated and they are grouped into bundles by astrocytes.[23,24] In species with larger eyes, such as humans and other primates, the opening in the sclera through which the axons leave the globe is fortified by the collagenous lamina cribrosa.[25,26] Small rodents possess only a rudimentary lamina cribrosa, or, in the case of mice, none at all.[27,28] However, whether or not a collagenous lamina is present, the ganglion cell axons are in direct contact to optic nerve astrocytes, a specialized subtype of white matter astrocyte.[24,29] Astrocytes perform several important functions for the neurons they support.[30,31] In the optic nerve, there is evidence that astrocytes are involved in calcium buffering[32] and fluid transport via a glymphatic pathway,[33] and may act as a part of the eye's pressure-sensing mechanism.[34,35] Recently, optic nerve astrocytes were also shown to be highly phagocytic,[36] aid in the degradation of myelin during development,[37] and relieve ganglion cell axons of degenerating mitochondria.[38] All of these functions could be impaired by aging.

Here we present a study of optic nerves from naïve C57bl/6 mice at various ages, ranging from young adulthood to near the end of the normal life span, and compare them to nerves from young mice that had experienced 1 month of elevated IOP.

Materials and Methods

Animal Husbandry

All animal studies were carried out in accordance with the ARVO Statement for the Use of Animals in Ophthalmic and Vision Research and were approved by the Institutional Animal Care and Use Committee of the Schepens Eye Research Institute. C57bl/6 mice from Jackson Laboratory (stock number 000664; Bar Harbor, ME, USA) were group housed under 12-hour dark and light cycles and received water and food at libitum. Eight-week-old C57bl/6 mice were adopted for the injection of microbeads and killed 4 weeks after the procedure (i.e., they were 12 weeks old at the time of euthanasia). Twelve- and 40-week-old naïve C57bl/6 mice were directly euthanized. An additional 15-, 18-, 27-, and 30-month-old C57bl/6 mice were retired breeders from our colony at the Schepens Eye Research Institute, but originally came from the same Jackson Laboratory stock.

Microbead Injection

Ocular hypertension was induced via microbead (15-μm diameter; Invitrogen, Carlsbad, CA, USA) injection into the anterior chamber as previously described.[39,40] Briefly, 2-month-old C57BL/6J mice were anesthetized by intraperitoneal injection of ketamine and xylazine, supplemented by topical proparacaine. The cornea of the right eye was gently punctured by a 30.5-gauge needle paracentrally, and 1.5 to 2.5 μL microbeads were injected into the anterior chamber with a glass micropipette connected to a Hamilton syringe (Reno, NV, USA). IOP was measured under light isoflurane anesthesia using a TonoLab rebound tonometer (ICare, Espoo, Finland) 1 day before the operation and twice weekly for 28 days following surgery. All measurements were conducted at the same time of the day. Five individual measurements were taken from each eye and the average was calculated.

Tissue Preparation and Sectioning

Mice were killed by CO_2 inhalation and perfusion fixation with 4% paraformaldehyde. The eyes and optic nerves were dissected free from the surrounding tissue. The optic nerves were embedded in 6% agarose, and 200-μm sections were cut on a Leica VT1000S vibratome (Buffalo Grove, IL, USA). The tissue sections were supported by nitrocellulose filters and postfixed in half-strength Karnovsky's fixative overnight at 4°C.[41]

Paraphenylenediamine Staining

The myelinated segments of optic nerves were fixed, dehydrated, and embedded in epoxy resin. Semithin (0.5 μm) sections were acquired using a Leica EM UC5 ultramicrotome and stained with a solution of 1% paraphenylenediamine (PPD) in 1:1 isopropanol:methanol. Tiling images of the whole nerve were taken on an Olympus BX51 microscope Center Valley, PA, USA) at ×40 magnification. The raw images were automerged using Adobe Photoshop CS6 (San Jose, CA, USA).

Transmission Electron Microscopy

The vibratome sections of the optic nerve heads were processed for electron microscopy as described previously.[41] We first prepared transverse sections of each optic nerve head. For one nerve in each group, the remainder of the tissue block was then re-embedded and longitudinal sections were cut from the same tissue. Images were taken on a FEI Tecnai G2 Spirit transmission electron microscope (FEI, Hillsboro, OR, USA) at 80 kV with an AMT XR41 digital CCD camera (Advanced Microscopy Techniques, Woburn, MA, USA).

Data Analysis and Statistics

Total axons were counted in 16 eyes from eight naïve young mice in the optic nerve proper after PPD staining using the AxonJ plugin in ImageJ.[42] The reliability of AxonJ counts was tested by manually recounting 10 fields containing 1280 axons on average. There was no significant difference between the counts obtained with AxonJ and a human observer ($P = 0.96$); the average difference in counts was 4.2% (range, 1.7%–10.2%). For transmission electron microscopy (TEM), naïve C57bl/6 mice at 3, 10, 15, 18, 27, and 30 months of age were used ($n =$ 4 eyes from 4 different animals for the 3-month group; $n = 2$ eyes from 2 different animals for 10 months; $n = 2$ eyes from the same animal for 15 months; $n = 1$ for 18 months [1 of the 18-month nerves was lost during preparation]; $n = 3$ from 2 different animals for 27 months; and $n = 2$ eyes from the same animal for 30 months). One additional 27-month-old nerve was sectioned longitudinally. The nerves were imaged with TEM in the glial lamina region (unmyelinated part of the nerve). Survey images of the whole nerve were taken at low magnification, followed by a sequence of 10 to 15 images around the midperiphery of the nerve and 2 or 3 images in the center at ×18,500 final resolution. The images were centered on axon bundles. The area of each of these fields was 36.652 μm^2. Blood vessels were imaged individually at ×6800 or ×9300 magnification. After TEM, individual optic nerves received a number code and the images were imported into ImageJ (version 1.50g; National Institutes of Health, Bethesda, MD, USA). Measurements were taken by an observer ignorant of the age and treatment condition of the mouse from which the nerve originated. All axons and mitochondria were counted in each image. The diameter of axons and mitochondria was measured in ImageJ. To avoid sampling bias, all axons and mitochondria that were completely contained in the image were measured. The thickness of the basement membrane was measured in eight positions around the perimeter of the vessel and averaged (Supplementary Fig. S1). The collagen profiles in the basement membrane were outlined in ImageJ and calculated as a percentage of the whole basement membrane. (Supplementary Fig. S2 shows collagen fibrils in various orientations at high magnification.) For measurements of basement membrane thickness and collagen content, only blood vessels that were sectioned perpendicularly to the long axis were considered. For the quantification of vesicles, the basement membranes of blood vessels were outlined and measured with ImageJ. Then astrocytic vesicles adjacent to the basement membrane were counted manually. The areas of the optic nerves were measured from tiled reconstructions of the whole nerve taken at ×2900 (Supplementary Table S1). The glial coverage in each nerve was measured by manually delineating the glial elements in medium- and high-power images. Total axons per nerve were calculated from the axon counts on the ×18,500 images and the total nerve area corrected for the glial components (a detailed description is given in the legend to Supplementary Table S2). Data were imported into Matlab (The Mathworks, Natick, MA, USA) for statistical analysis. Differences between groups were tested with ANOVA or a Kruskal-Wallis test followed by a Mann-Whitney test. Figures are given as mean ± standard deviation.

Data Sharing

Original TEM images were deposited to the Harvard Dataverse and can be viewed or downloaded under https://dataverse.harvard.edu/dataverse/AgedOpticNerve.

Results

Total Axon Counts in Young Naïve C57bl/6 Mice

In a preliminary experiment we counted axons in 16 naïve optic nerves from 3-month-old C57bl/6 mice ($n = 16$ nerves, from 3 female and 5 male mice) to estimate how much natural variety in axon counts occurs even in age-matched individuals from the same strain and distributor. The average axon count was 41,582 ± 5671, and there was no significant difference between male and female mice (Supplementary Fig. S3A). The axon counts in this group varied considerably (range, 30,182–50,103), and the left and right eyes of the same animal did not correlate closely ($R^2 = 0.24$, $n = 8$; Supplementary Fig. S3B).

Age- and IOP-Related Changes in the Axons of the Glial Lamina

We studied the ultrastructural morphology of the glial lamina (Figs. 1A, 1B) in naïve C57bl/6 mice of various ages from young adulthood (3 months) close to the end of the natural life span of mice (30 months). All sections were obtained from the glial lamina of the optic nerve head, between the myelination transition zone and the prelaminar region (dashed lines in Figs. 1A, 1B indicate the plane of section). Figures 1C through 1F show representative images from 3-, 10-, 18-, and 30-month-old nerves (images from 15- and 27-month-old nerves are shown in Supplementary Figs. S4A–C). We also induced elevated IOP in four young C57bl/6 mice for 1 month so that the animals were 3 months of age at the end of the experiment (Supplementary Fig. S5). Representative images of these nerves are shown in Figure 2. The total area of the nerve was determined from tiling medium-power images, and the axon packing density was calculated for every nerve (Supplementary Table S1).

The axon packing density of naïve mice decreased slightly with age; however, as shown in Figure 3A, the correlation was only moderate ($R^2 = 0.56$, $P = 0.0022$). Total axon counts per nerve showed a strong inverse correlation with age (Fig. 3B, $R^2 = 0.75$, $P = 5.5E\text{-}5$). Mean axonal diameters correlated moderately with age (Fig. 3C, $R^2 = 0.71$, $P = 0.00017$), and the axon diameters in the 30-month-old group were significantly larger than those in the 3-month group ($P = 3.71E\text{-}9$). However, the modes of the axon diameters in the old and glaucomatous groups were smaller than those in the 3-month group (Table). As is visible in Figures 1C through 1F, old nerves are characterized by the simultaneous occurrence of well-preserved axons with normal interior structure and enlarged axons that appear pale and have lost neurofilaments and most of the microtubules. The variance of axonal diameters showed the closest correlation with age of all measurements (Fig. 3D, $R^2 = 0.89$, $P = 5.47E\text{-}7$). Axonal size distributions indicate that in young naïve nerves the mode of the distribution is 0.3528 μm and axon diameters larger than 1.5 μm are rarely encountered. In aged nerves progressively more enlarged axons are found (Figs. 1C–F; see also Supplementary Fig. S6 for lower-power images, and Supplementary Fig. S7 for distribution histograms of each age group). Nerves that were subjected to 1 month of elevated IOP to the naïve nerves showed changes that were similar to those observed in aged nerves. In particular, the variance of axonal diameters was similar to those in nerves over 18 months of age (Fig. 3D).

We next asked whether the increased variance of axonal diameters in aged and glaucomatous nerves was caused by the simultaneous presence of two sets of axons, one morphologically normal and the other showing pale axoplasma and increased diameter, or whether it was caused by more localized swelling of axons during their course through the glial lamina.

We therefore imaged longitudinal sections taken from the same optic nerve heads after re-embedding. As shown in Figure 4, individual axons had both narrow segments with normal axoplasm and enlarged segments with no or very few cytoskeletal elements. Within these swellings, there were always mitochondria. These variations in axon caliber were present even in nerves of young naïve mice (Fig. 4A), but increased in numbers and size in aged and in glaucomatous nerves (Figs. 4B–E).

Changes in Mitochondria

In the glial lamina of young naïve mice, approximately 0.3 profiles of mitochondria were encountered per axonal profile (Fig. 5A). Astrocytic mitochondria were more electron dense and usually larger than axonal mitochondria (Fig. 5B), which may be indicative of a high energy output.[43] In addition, some axons contained mitochondrial profiles that showed various degrees of pathology. We graded mitochondria from all age groups and the microbead-injected group. Grade I correspond to morphologically normal mitochondria whose cristae fill out the whole profile. Grade II show a decreasing density of cristae, but >50% of the mitochondrion still is filled with cristae. Grade III additionally have inclusion bodies inside. Grade IV mitochondria are <50% filled with cristae, and grade V are completely empty, but still have a double membrane. In addition, axons occasionally contained multilamellar structures and mitochondria that contained vacuoles (Fig. 6A). In young nerves, 76% of the mitochondria were grade I or II, but higher grades were increasingly numerous in in older and glaucomatous nerves (Fig. 6B). At the same time, the astrocytic mitochondria appeared morphologically normal even in very old and glaucomatous nerves (Fig. 5D). We measured the diameters of mitochondria (except those completely without cristae and multilamellar bodies) in cross sections (Supplementary Table S3). In the 3-month group, the mean mitochondrial diameter was 0.3807 ± 0.1552 μm ($n = 1867$). The mitochondrial diameters were significantly enlarged in all aged nerves and in the glaucoma group (10 months, 0.4207 ± 0.1893 μm, $n = 877$, $P = 5.75E\text{-}8$; 15 months, 0.4402 ± 0.1969, $n = 603$, $P = 3.71E\text{-}8$; 18 months, 0.4183 ± 0.201 μm, $n = 374$, $P = 3.76E\text{-}4$; 27 months, 0.5436 ± 0.2226, $n = 704$, $P = 3.71E\text{-}8$; 30 months 0.4688 ± 0.2189 μm, $n = 704$, $P = 3.71E\text{-}8$; microbeads, 0.4576 ± 0.1815 μm, $n = 1243$, $P = 3.71E\text{-}8$). The variance of axonal mitochondria diameters correlated well with age (Fig. 6C, $R^2 = 0.78$, $P = 2.89E\text{-}5$).

We also measured the diameter of the axonal mitochondria in longitudinal sections. The mean diameters in the 3-, 10-, 18-, and 30-month-old naïve groups were 0.528 ± 0.230 μm ($n = 99$), 0.659 ± 0.262 μm ($n = 27$, $P = 0.15$, not significantly different from 3-month group), 0.613± 0.267 μm ($n = 53$, $P = 0.327$), and 0.699 ± 0.306 μm ($n = 110$, $P = 3.12E\text{-}5$), respectively. The mean longitudinal mitochondrial diameter of microbead-injected young mice was 0.671 ± 0.214 μm ($n = 37$, $P = 0.0394$).

Blood Vessels of the Glial Lamina

Thin sections through the glial lamina usually contained five to eight individual profiles of the blood vessel plexus in the nerve head. The vessel walls contained no smooth muscle cells, but occasionally pericytes were visible. In each case, the vessel was completely surrounded by astrocyte endfeet (Figs. 7A–C). In 3-month-old nerves, the basement membranes were on average 0.361 ± 0.244 μm thick, the average basement membrane area was 10.683 ± 6.828 μm^2, with 8.442 ± 8.365% of the basement membrane area taken up by collagen fibrils ($n = 16$ blood vessels). In 10-month-old nerves, the basement mem-

Investigative Ophthalmology & Visual Science

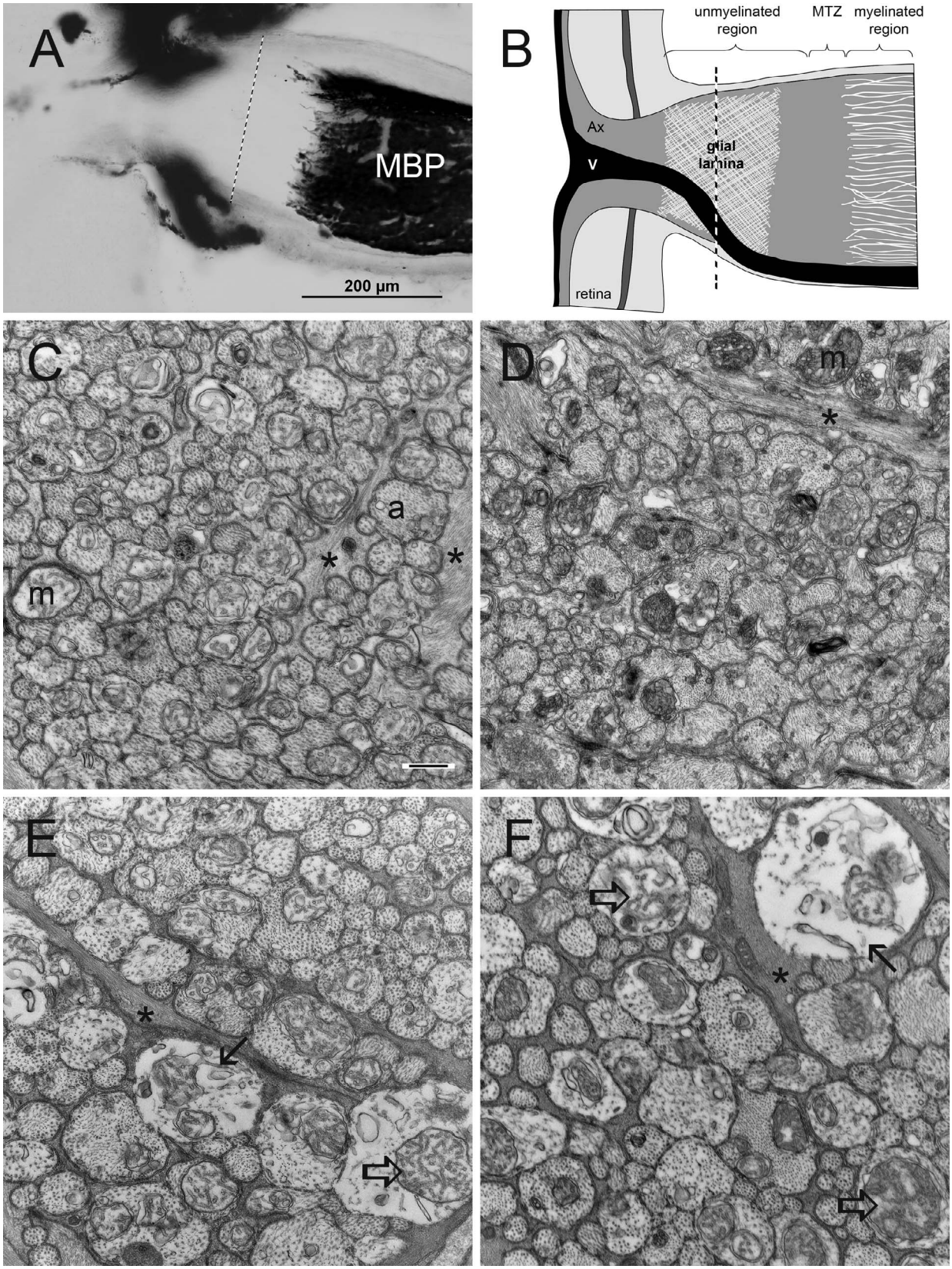

Figure 1. Axonal enlargement and mitochondrial swelling in the aging murine optic nerve head. (**A**) Light microscopic image of the optic nerve stained for myelin basic protein (MBP), the *dotted line* shows the plane of section for the electron microscopic images in (**C**–**F**). (**B**) Schematic diagram of the optic nerve head, the *dotted line* shows the plane of section. (**C**–**F**) Optic nerve cross sections in transmission electron microscopy: (**C**) 3 months old; (**D**) 10 months old; (**E**) 18 months old; (**F**) 30 months old. m: mitochondria; a: axons; *asterisks*: astrocytic processes. The *solid arrows* in (**E**, **F**) highlight examples of enlarged axons, and *open arrows* in (**E**, **F**) indicate swelling and degenerating mitochondria. *Scale bars*: 200 µm (**A**); 0.5 µm (**C**).

Investigative Ophthalmology & Visual Science

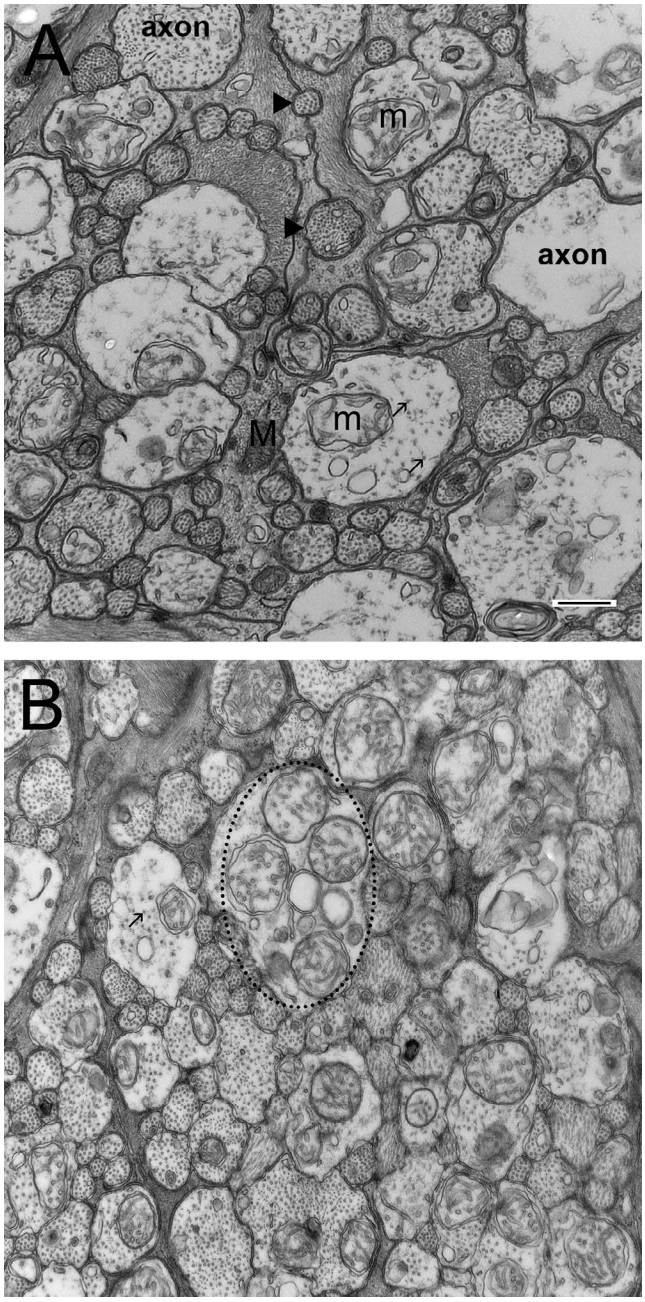

Figure 2. Axons and axonal mitochondria are enlarged and degenerated in ONHs of young microbead-injected mice. (**A**) *Arrows* point to microtubules. *Solid triangles* indicate normal axons. m: axonal mitochondria; M: astrocytic mitochondria. (**B**) *Dotted circle* shows the cluster of mitochondria and mitochondria without cristae in the abnormal axon. *Scale bar*: 0.5 μm.

branes were significantly thicker (1.678 ± 0.729 μm, $n = 19$, $P = 5.31E\text{-}7$); the area covered by the basement membrane was larger (34.708 ± 21.423 μm, 4.33E-4) and contained more collagen (28.344 ± 14.718%, $P = 2.46E\text{-}4$). In very aged mice (27 and 30 months old), the mean basement membrane thickness was still increased compared to the 3-month group (1.499 ± 0.623 μm, $n = 12$, $P = 5.24E\text{-}5$), though there was no further increase compared to the 10-month group ($P = 0.988$). As a tendency, blood vessels in glaucomatous nerves fell in the middle (0.814 ± 0.607-μm thickness, $P = 0.119$; 14.875 ± 12.369-μm^2 area, $P = 0.854$; 19.016 ± 13.7% collagen, $P = 0.068$; $n = 24$). This was not significantly different from the naïve control group (Figs. 7D–F).

The cell membrane of the astrocyte endfeet around the blood vessels contained multiple invaginations, caveolae, and adjacent vesicles (Figs. 8A, 8B). We quantified the number of caveolae in young and aged nerves and in nerves after elevation of IOP. In young nerves, there were 1.06 ± 0.33 caveolae per 1 μm of membrane ($n = 16$), which was reduced to 0.75 ± 0.31 in 10-month-old nerves ($n = 18$, $P = 0.023$); and it was 0.76 ± 0.16 in 27- to 30-month-old nerves ($n = 30$, $P = 0.048$). Glaucomatous nerves were not significantly different from the controls (Fig. 8C, 1.38 ± 0.55 caveolae/μm, $n = 17$, $P = 0.55$, NS).

Regional Differences Within Glaucomatous Optic Nerve Heads

In prior studies, the damage to ganglion cell axons was reported to be more severe in the dorsal part of the nerve,[29,43,44] corresponding to the superior half of the retina. We imaged the glaucomatous optic nerves at low magnification to screen for regional differences in axon pathology. Though enlarged axons and abnormal mitochondria are present throughout aged and glaucomatous nerves, the highest numbers are found around the dorsal and lateral rim (Fig. 9A), whereas axon bundles close to the ventral side appear to be relatively protected. Neither in the dorsal nor the ventral part of the nerve did we observe astrocyte processes that had retracted or were no longer inserted in the pia (Fig. 9A). We did find enlarged axon segments filled with mitochondria close to or inside astrocyte processes. These structures were most common around the dorsal and lateral rim (Fig. 9B), but they were present throughout the whole nerve (Fig. 9A).

Discussion

The maximum life expectancy of C57bl/6 mice in captivity is approximately 36 months, but the maturation rate of mice does not directly map onto that of humans.[45] In infancy and youth, mice age approximately 150 times faster than humans until they reach reproductive maturity. The maturation rate slows down to approximately 45 times until the mice approach reproductive senescence, and slows down to approximately 25 times at ages older than 6 months.[46] A mouse would be comparable to a young adult human at 3 to 6 months, to a middle-aged human at 10 to 14 months, and to an old human at ages 18 months and older.[46] This consideration prompted the choice of age groups in this study. At 3 months, the retina and optic nerve of mice are fully mature and the mice are in their young age, so these nerves serve as the baseline of comparison. The age of 10 months corresponds to the human age where the incidence of glaucoma starts to rise.[47] The oldest nerves in our sample (27 and 30 months) were included to find how far age-related changes in the optic nerve progress in the absence of glaucoma.

In the glial lamina of the optic nerve, the hallmarks of age-related changes are (1) a reduction in axon packing density and the total number of axons per nerve; (2) an increase in the variance of axon diameters; (3) obvious signs of mitochondrial pathology; and (4) a thickening of the blood vessel basement membranes and increased collagen deposition. One month of moderately increased IOP mimics the effects of at least 1 year of normal aging on the morphology of optic nerve axons and mitochondria.

Estimates of axon loss throughout aging are complicated by the relatively high variability in axon counts even in strain-matched animals and the variability between sample areas from

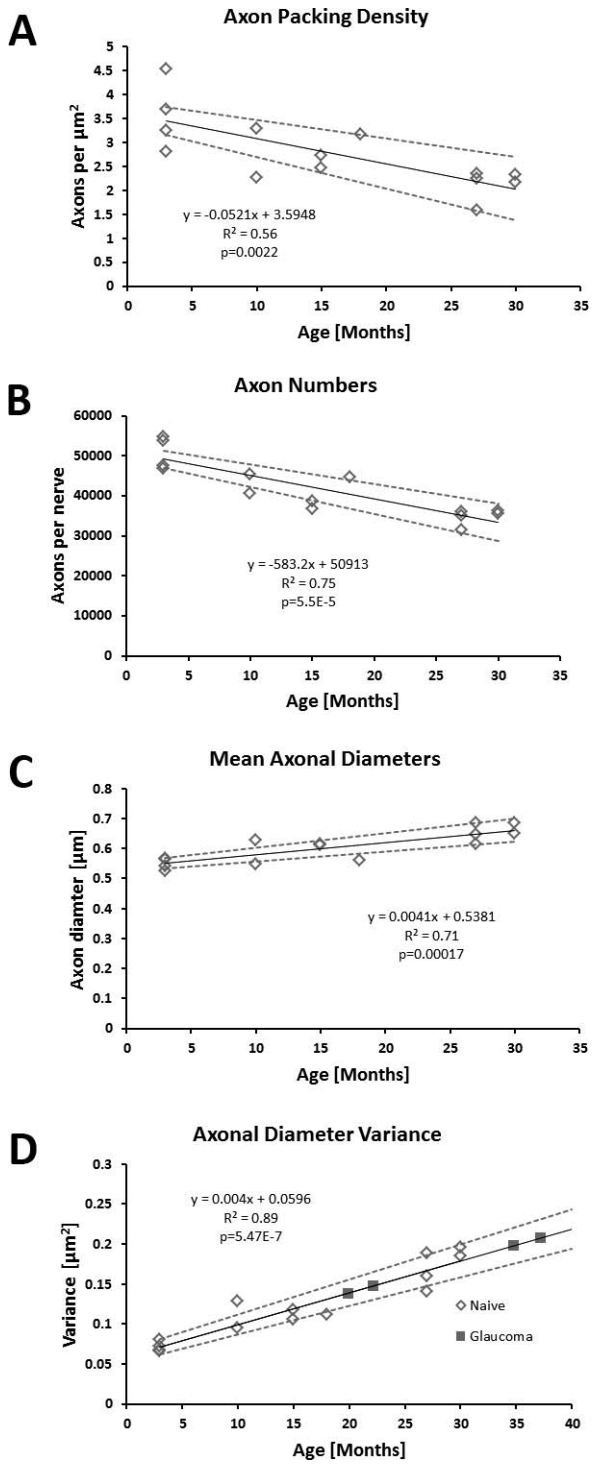

Figure 3. Axons swell with age, and young glaucomatous ONH showed an aged appearance. Every data point in this figure represents one optic nerve. The numbers for age groups were not averaged before correlation analysis. (For an analysis based only on one eye per animal, see Supplementary Fig. S8.) (**A**) Axon packing density decreases with age. (**B**) Total axon counts per nerve decrease with age. (**C**) Axon diameters slightly increase with age. (**D**) Variance of axonal diameter increases and highly correlates with age. The linear regression model was based on the naïve mice alone (*open diamonds*). The linear regression line is indicated as a *solid gray line*. Confidence ranges for the linear regression model are given by *dashed lines*. The parameters for the linear regression, R^2, and P for the correlation are indicated in each part of the figure. Superimposed on the graph in (**D**) is the variance of axon diameter in the glaucoma group (*solid squares*).

the same nerve.[48] Yet, most, though not all,[49–51] studies in various species, including humans, report a steady ganglion cell and axon loss during the lifetime.[48,52–56] In the present study, we calculated total axon numbers per nerve by measuring area, axon packing density, and glial coverage for every nerve (see Supplementary Table S2). Our measurements are consistent with an axon loss of 583 ± 96 fibers per month, or roughly 7000 per year. This is similar to the rate reported for humans (approximately 4000 per year),[54] and slightly lower than that reported for mouse ganglion cells using retrograde labeling (2.3% per month).[57]

Though mean axonal diameters showed an age-dependent increase, the distribution of diameters did not simply shift to the right in older nerves. Rather, we observed the simultaneous occurrence of small axons with well-preserved internal structure and cytoskeleton, an age-dependent increase in very large axons with pale axoplasm, and, very often, accumulations of abnormal mitochondria. A possible interpretation would be that there are different populations of axons, one fairly normal or resilient, and a second with pathological changes. Longitudinal sections of the same nerves showed that this was not the case. Individual axons that could be traced through the glial lamina had both narrow segments with normal internal structure and enlarged segments without clearly identifiable cytoskeleton that usually also contained abnormal mitochondria. The occurrence of enlarged segments with accumulations of mitochondria is not pathological per se, as it is observed in young animals (Fig. 4A) and has been described in retinal axon fibers in other species, too.[58] However, there is a strong age-dependent increase in caliber variance and the occurrence of swellings (Figs. 3D, 4B–E). A similar increase is observed in young nerves after 1 month of IOP elevation, which makes these nerves appear morphologically older than they actually are (Fig. 3D).

Axonal swelling in the glial lamina could be explained by a disruption of axonal transport. Axonal tracers have a tendency to accumulate in the glial lamina and the myelination transition zone even in young healthy animals, and elevated IOP is known to interfere with axonal transport.[21,59–62] Alternatively, axonal damage may be caused by mitochondrial dysfunction, a relative lack of adenosine triphosphate (ATP), or leakage of reactive oxygen species and nucleotides from the damaged mitochondria. In our sample, abnormal axon segments often contained clusters of enlarged mitochondria or mitochondria with few cristae. Axonal transport is dependent on actin and microtubule tracks, and on ATP, so mitochondrial damage would certainly affect axonal transport as well.[63]

Recently, several reports have implicated mitochondrial dysfunction in age and glaucomatous optic nerve damage.[14,64–66] Age and glaucoma were reported to lead to a decrease in the ATP levels in the optic nerve[11] and to a reduction in mitochondrial density.[12] Conversely, particularly efficient mitochondria confer resistance to optic neuropathy,[67] and targeting mitochondrial function is a potential therapeutic approach to glaucoma.[68,69] Working with the DBA/2J strain of mice, a common model of hereditary glaucoma, several recent studies have identified mitochondrial pathology in the myelinated and unmyelinated segments of the optic nerve on the ultrastructural level.[13,70–72] Some of the reported findings—namely, the increase in mitochondria with abnormal or absent cristae—are similar to our observations in aged and glaucomatous C57bl/6 mice. However, in contrast to the studies in glaucomatous DBA/2J mice, we find an overall enlargement of

Though the glaucomatous mice were only 3 months old, considering the variance of axonal diameters their apparent "ages" were at least 18 months.

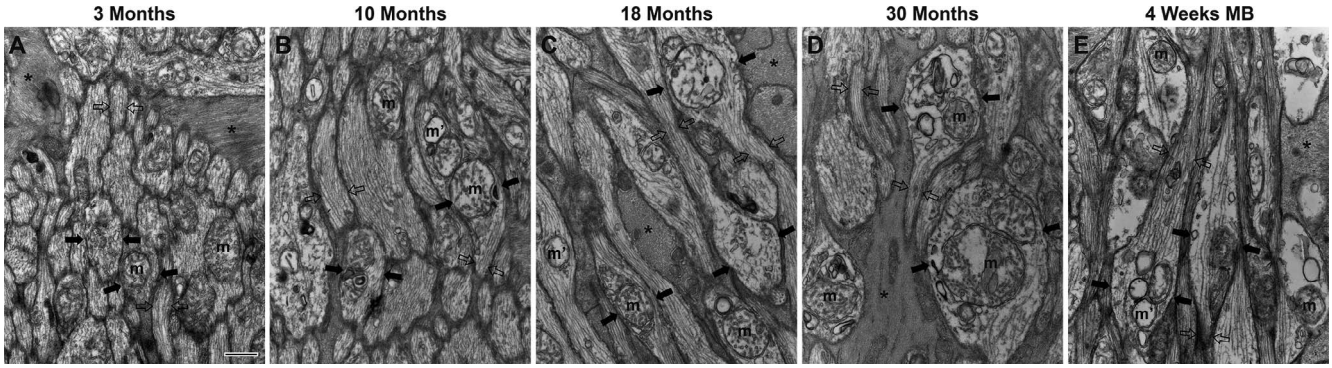

FIGURE 4. Longitudinal sections showing increased incidence of swollen axonal segments and abnormal mitochondria in the aged and glaucoma groups. Both enlarged and normal slim segments are present in the same axons. Most of the enlarged parts of the axons contain swollen mitochondria. (**A**–**D**) Longitudinal sections of 3- to 30-month-old naïve ONHs under TEM. (**E**) Longitudinal section of 4-week microbead-injected young ONH. *Solid black arrows* point to enlarged segments of axons and *open black arrows* show normal slim segments of axons. m: relatively normal mitochondria; m': mitochondria without cristae; *arrowheads* show mitochondria without cristae. *Asterisk* identifies the astrocyte processes. *Scale bar*: 500 nm.

mitochondria. However, we did not include mitochondria without cristae (grade V) or multilamellar bodies (which most likely correspond to autophagosomal remnants of mitochondria) in our measurements, which may explain the discrepancy. It should be noted that the changes in mitochondrial structure are a matter of degree. Abnormal mitochondria, including those without cristae, are present even in 3-month-old samples. However, they are more commonly encountered

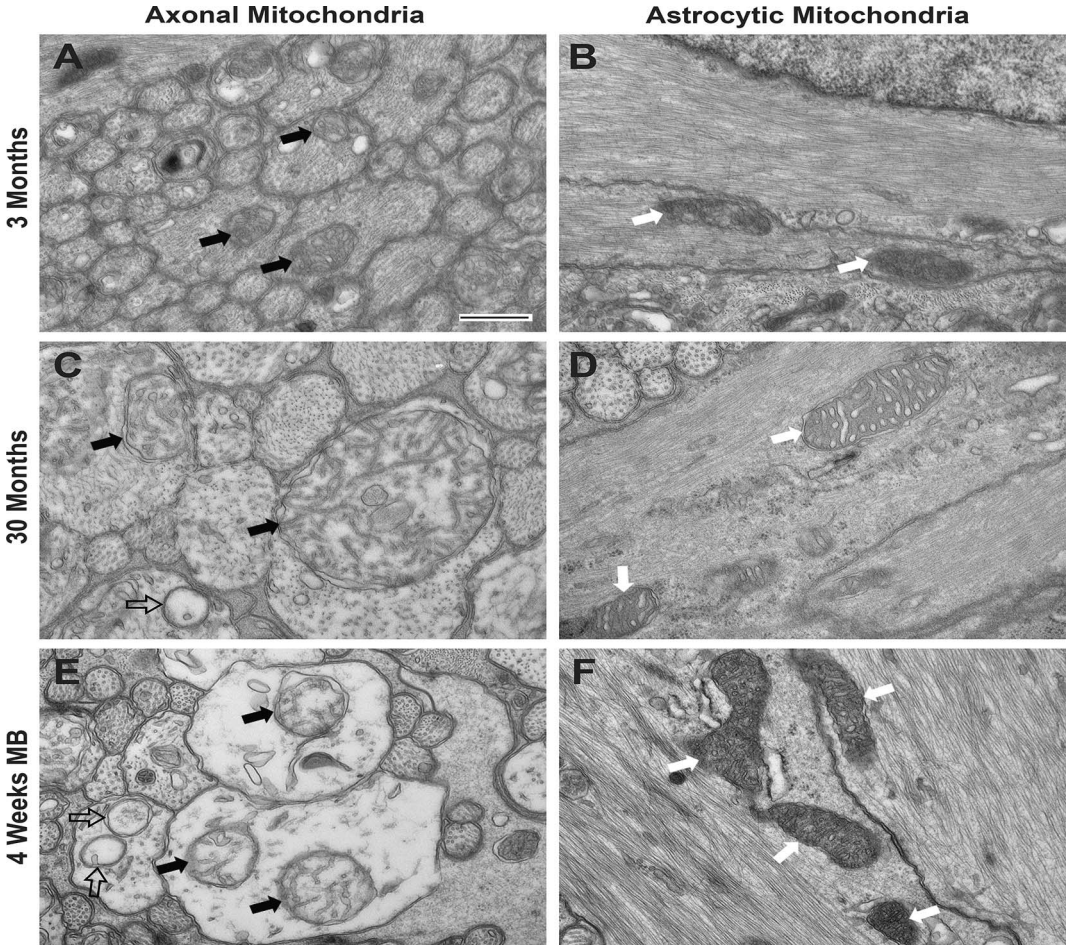

FIGURE 5. Axonal mitochondria swell and degenerate in aged ONHs and ONHs of microbead-injected mice while astrocytic mitochondria remain intact. *Black solid arrows* indicate axonal mitochondria; *black open arrows* indicate mitochondria without cristae, and *white arrows* indicate astrocytic mitochondria. (**A**) 3-month naïve ONH axons; (**B**) 3-month naïve ONH astrocyte processes; (**C**) 30-month naïve ONH axons; (**D**) 30-month naïve ONH astrocyte processes; (**E**) 3-month ONH axons of 4-week microbead-injected mice; (**F**) 3-month ONH astrocyte processes of microbead-injected mice. *Scale bar*: 0.5 μm.

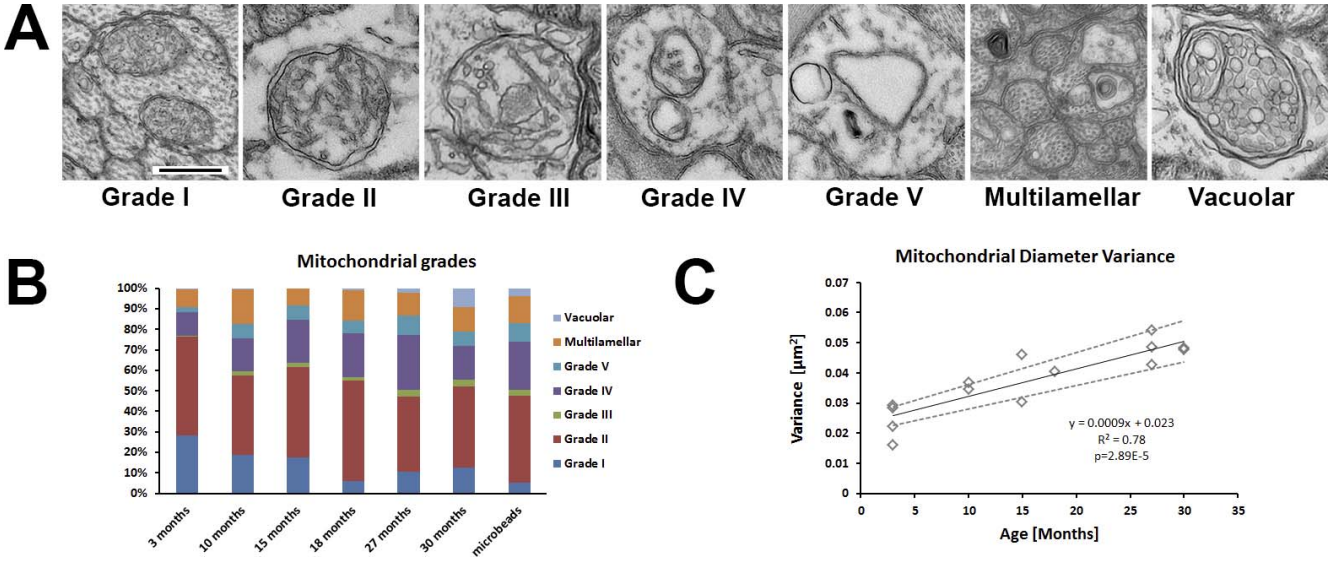

Figure 6. Mitochondria show various grades of pathology. (**A**) Grade I correspond to mitochondria that are completely filled with cristae; grade II show some loss of cristae, but are still filled to >50%; grade III mitochondria additionally contain inclusion bodies; grade IV mitochondria have lost all but a few cristae; and grade V mitochondria are devoid of cristae, but still have a double membrane. There are also multilamellar bodies and mitochondria that appear to have large vacuoles. *Scale bar*: 500 nm for all parts of (**A**). (**B**) Bar graph showing the population of mitochondria by grade as a percentage of the whole population encountered in this group. (**C**) Mitochondrial diameter variance increases with age. *Open diamonds* represent the variance for each nerve. The *dotted lines* indicate the confidence range of the regression line.

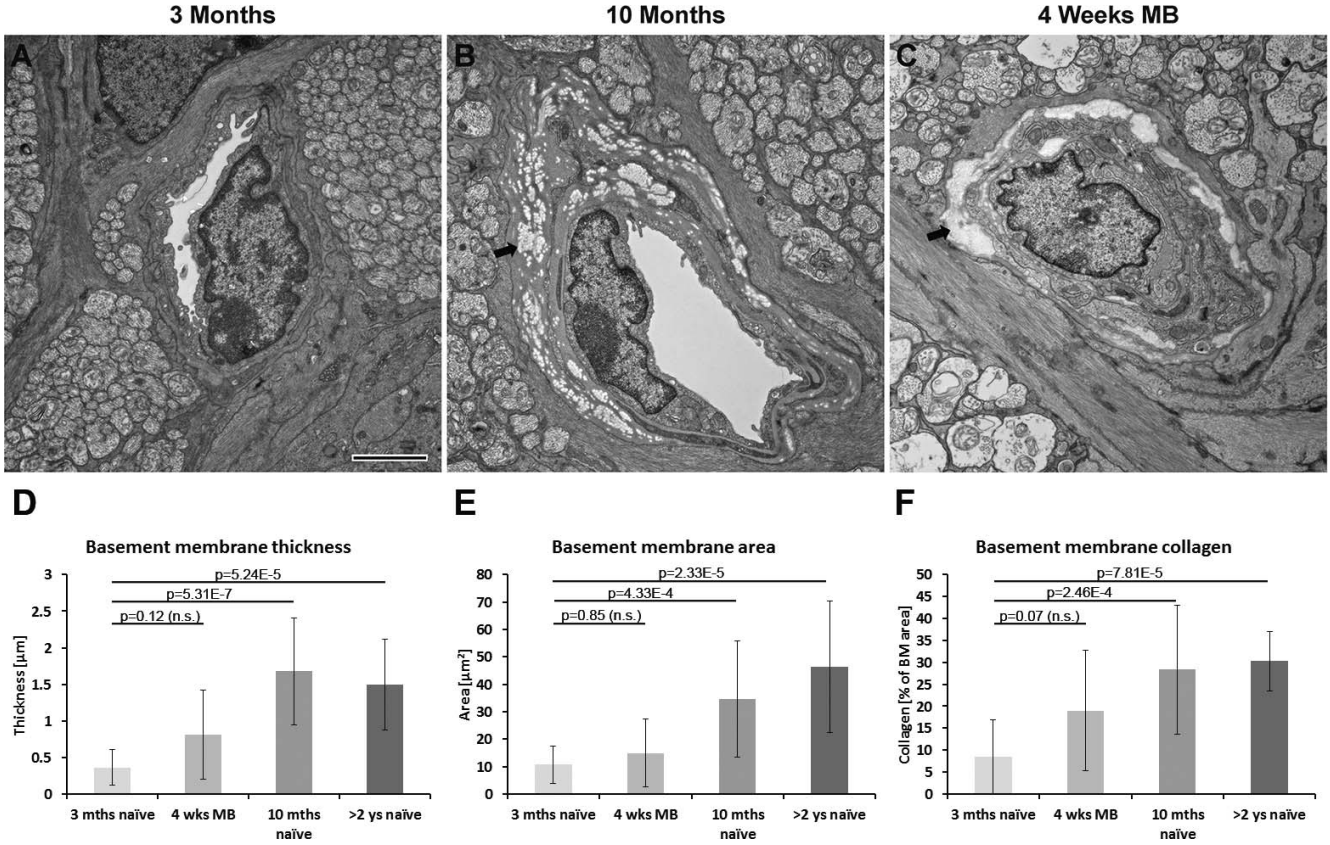

Figure 7. Basement membrane thickening and collagen deposition in old naïve blood vessels and glaucomatous blood vessels. (**A–C**) Electron microscopic images of blood vessels in 3-month naïve, 10-month naïve, and 4-week microbead-injected young ONHs ($n = 19$). *Black arrows* point to collagens fibrils. *Scale bar*: 2 µm. (**D**) Quantification of basement membrane thickness in 3-month-old naïve ($n = 16$), microbead-injected ($n = 24$), 10-month-old naïve ($n = 19$), and >2-year-old naïve ($n = 12$) ONHs. (**E**) Quantification of basement membrane areas in 3-month, microbead-injected, 10-month, and >2-year-old ONHs. (**F**) Percentage of basement membrane occupied by collagen in 3-month, microbead-injected, 10-month, and >2-year-old ONHs.

Investigative Ophthalmology & Visual Science

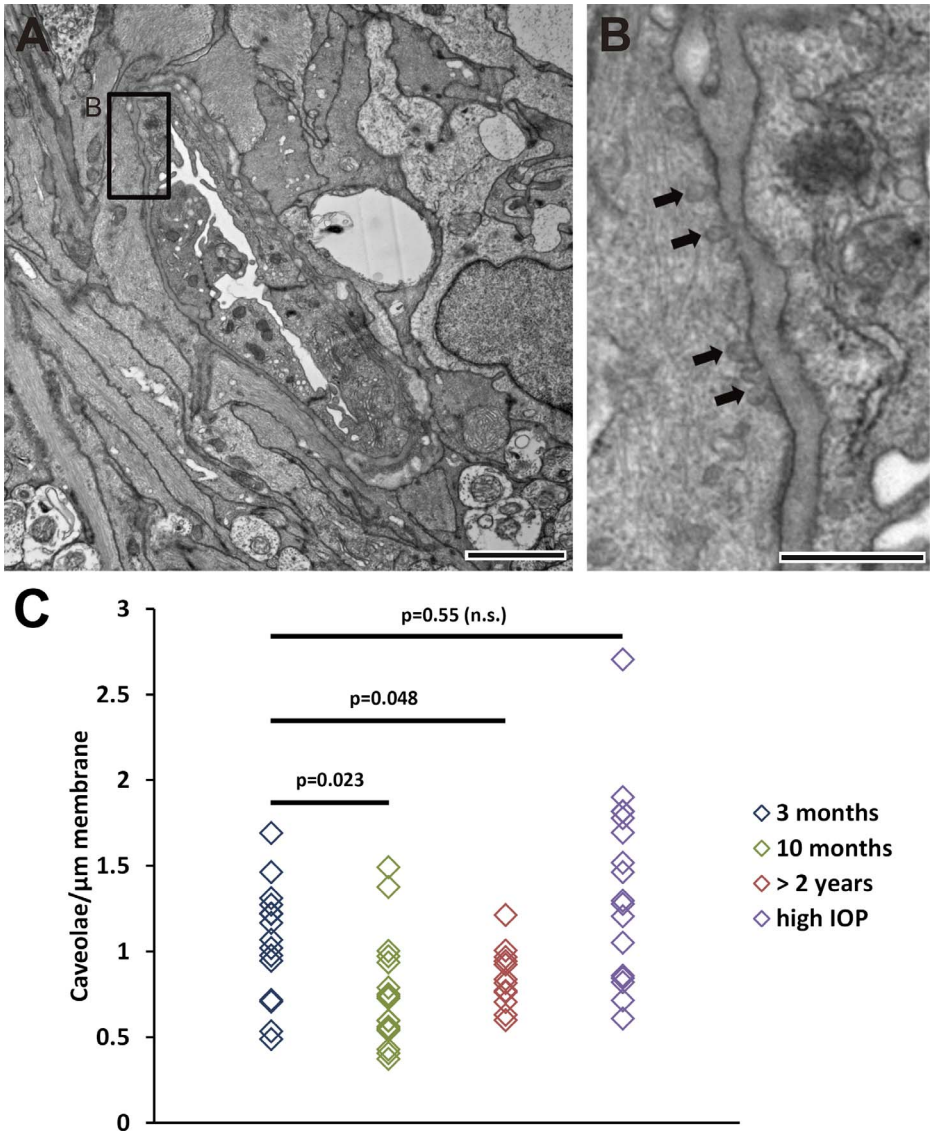

Figure 8. Caveolae are decreased in aged ONHs but not in glaucomatous ONHs. (**A**) Blood vessel in 3-month naïve ONH. (**B**) Higher-power view of the *boxed area* in (**A**). The cell membrane of the astrocyte endfeet around the blood vessels contained multiple invaginations, caveolae, and adjacent vesicles. *Black arrows* point to caveolae. (**C**) Caveolae counts per membrane in aged ONHs are decreased in aged mice; caveola counts in young nerves 4 weeks after microbead injection are not different from the young naïve group. *Scale bars*: 2 µm (**A**); 0.5 µm (**B**).

in aged and glaucomatous nerves.[13] A possible interpretation is that mitochondrial enlargement precedes their degeneration and degenerating mitochondria persist if they are not cleared by mitophagy. In the glial lamina, astrocytes may be involved in this process. The astrocytes of the glial lamina, and in particular of the myelination transition zone, are phagocytic and aid in the transcellular degradation of axonal mitochondria.[36,38,41] In our samples, we also found axonal evulsions that

Table. Axonal Diameters, Variance, and Standard Deviation (Stdev) of Diameters, Median, and Mode for All Age Groups and the Microbead-Injected Group

Group	Number of Axons Measured	Mean Axon Diameter, µm	Variance Axon Diameter, µm^2	Stdev Axon Diameter, µm	Median Axon Diameter, µm	Mode Axon Diameter, µm
3 mo naïve	5412	0.5453	0.0716	0.2676	0.4742	0.3528
10 mo naïve	2279	0.5798	0.1098	0.3314	0.4840	0.3094
15 mo naïve	1954	0.6135	0.1119	0.3345	0.5210	0.4373
18 mo naïve	1256	0.5599	0.1114	0.3338	0.4520	0.2256
27 mo naïve	2487	0.6446	0.1605	0.4006	0.5223	0.2644
30 mo naïve	2170	0.6648	0.1898	0.4356	0.5050	0.2919
Microbeads	4081	0.5583	0.1698	0.4120	0.3944	0.2271

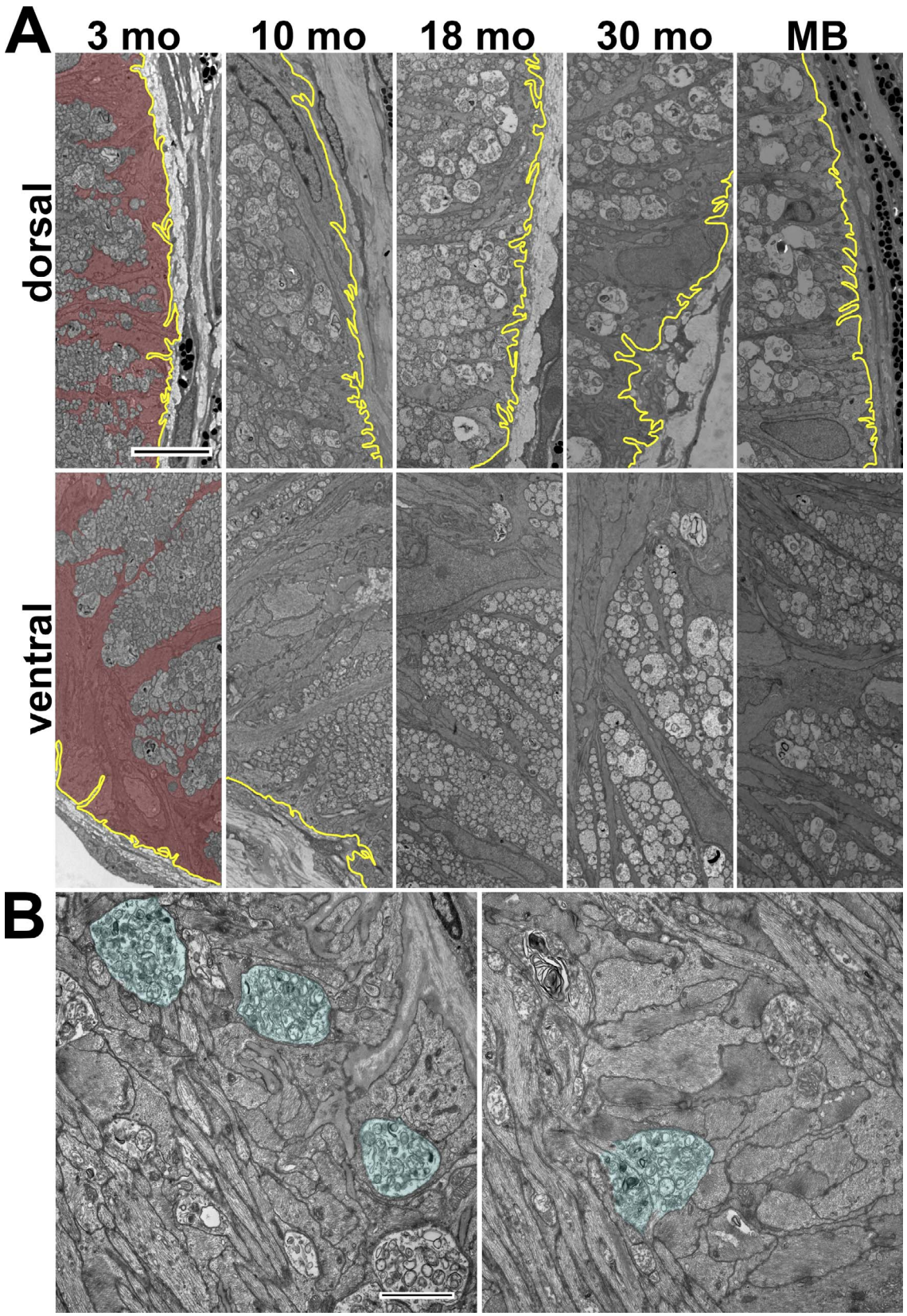

Figure 9. Axon damage was most pronounced in the vicinity of the dorsal and lateral surface of the nerve. (**A**) Low-power EM images of the dorsal and ventral part of optic nerve heads from 3-, 10-, 18-, and 30-month-old naïve and 4-week microbead-injected mice. More abnormal axons were observed in aged and microbead-injected optic nerve head. The dorsal part showed a more pronounced axonal damage than the ventral part. The astrocyte processes from 3-month-old optic nerve heads were false colored in *red*. *Yellow lines* outline pial walls of the optic nerve head. (**B**) Longitudinal sections from a 18-month-old nerve. The bag-like structures false colored in *blue* containing abnormal mitochondria were enwrapped in astrocytic processes. (These structures were particularly numerous close to the dorsal rim of the optic nerve.) *Scale bars*: 5 µm (**A**); 2 µm (**B**).

Investigative Ophthalmology & Visual Science

are filled with mitochondria and appear to be engulfed by astrocyte processes (Fig. 9B).

As the axons are myelinated only after approximately 400 μm behind the sclera, the glial lamina is expected to have a higher energy demand than the myelinated optic nerve proper.[73] Axons and glia of the optic nerve head rely for their blood supply on a plexus of vessels inside the nerve. During normal aging, the basement membrane of the blood vessels becomes thicker and incorporates more collagen (Fig. 7). Similar findings have been reported from human eyes with primary open-angle glaucoma.[16,74,75] A likely consequence is that the exchange of oxygen and nutrients is impeded in older nerves and the tissue is less able to satisfy its energy demand. In our sample of glaucomatous mice, the basement membrane was not significantly thicker than in the naïve age-matched group. This may be due to the relatively short time the eyes were subject to increased IOP (30 days). Whereas changes in axonal transport or astrocyte process orientation can occur within hours or days,[76–78] the thickening of the basement membrane would require the synthesis and deposition of new material.

In addition to axons and blood vessels, the optic nerve head is rich in astrocytes that are in direct contact to the axons.[23,24,79] Recent studies implicated the "fortified" astrocytes of the optic nerve head in the pathology of glaucoma.[29,43] Working in a rat model of ocular hypertension, Dai et al.[29] observed the development of fluid-filled extracellular spaces followed by a retraction of astrocyte processes in the dorsal part of the nerve and a loss of contact of astrocyte endfeet with the pial wall. Axons close to the dorsal surface degenerated first. This is compatible with the observation that in many rodent models of glaucoma the ganglion cell loss is more pronounced in the superior half of the retina, which is the origin of the axons that form the dorsal part of the nerve.[20,24,55,80] In our sample, we never found large extracellular spaces or astrocyte processes that had retracted in this region. This may be due to the fact that the IOP elevation in our animals was lower than that reported by Dai and colleagues (20.55 ± 3.9 vs. >40 mm Hg). Nevertheless, the axon damage in our sample was most pronounced in the vicinity of the dorsal and lateral surface of the nerve, suggesting that the astrocyte processes in this region are subject to increased stress.

Finally, it should be noted that electron microscopic studies have their limitations. Though our data are based on several hundred measurements of axons and mitochondria per individual nerve, the relatively slow sample preparation, imaging, and analysis process precludes studying large numbers of nerves per group. Since two eyes from the same animal show a slight correlation in axon numbers (Supplementary Fig. S3B), there is the possibility that a single animal significantly skews regression analyses (such as shown in Fig. 3) and leads to an overestimate of the correlation coefficients. To alleviate this concern, we reanalyzed all correlations including only those nerves that came from different individual mice ($n = 11$). As shown in Supplementary Figure S8, this did not change the conclusions. Still, due to the relatively low sample sizes typical of this type of study, the results should be interpreted with caution.

In conclusion, age- and IOP-induced changes in the optic nerve head involve the neural, glial, and vascular components. The morphologic similarities between age and glaucoma suggest that on the molecular level, too, there will be considerable overlap in gene expression patterns. Damage that accumulates in the optic nerve over time seems to be accelerated by elevated IOP so that glaucomatous nerves appear prematurely aged.

Acknowledgments

The authors thank Richard Masland for critically reading the manuscript, Scott Greenwald for advice on perfusion fixation, and Russell Woods for helpful discussions about statistical analysis.

Supported by National Institutes of Health Grant (NIH) R01EY019703, NIH Core Grant for Vision Research P30EY003790, and grants from the Chinese Scholarship Council. The authors thank the Massachusetts Lions Eye Research Fund, Research to Prevent Blindness, and the donors of National Glaucoma Research, a program of the BrightFocus Foundation.

Disclosure: **Y. Zhu**, None; **A.C. Pappas**, None; **R. Wang**, None; **P. Seifert**, None; **D. Sun**, None; **T.C. Jakobs**, Santen, Inc. (R)

References

1. Quigley HA. Glaucoma. *Lancet*. 2011;377:1367–1377.
2. Nickells RW, Howell GR, Soto I, John SW. Under pressure: cellular and molecular responses during glaucoma, a common neurodegeneration with axonopathy. *Annu Rev Neurosci*. 2012;35:153–179.
3. Libby RT, Gould DB, Anderson MG, John SW. Complex genetics of glaucoma susceptibility. *Annu Rev Genomics Hum Genet*. 2005;6:15–44.
4. Quigley HA, Broman AT. The number of people with glaucoma worldwide in 2010 and 2020. *Br J Ophthalmol*. 2006;90:262–267.
5. Guedes G, Tsai JC, Loewen NA. Glaucoma and aging. *Curr Aging Sci*. 2011;4:110–117.
6. Wiggs JL. The cell and molecular biology of complex forms of glaucoma: updates on genetic, environmental, and epigenetic risk factors. *Invest Ophthalmol Vis Sci*. 2012;53:2467–2469.
7. Caprioli J. Glaucoma: a disease of early cellular senescence. *Invest Ophthalmol Vis Sci*. 2013;54:ORSF60–ORSF67.
8. Wilson AM, Di Polo A. Gene therapy for retinal ganglion cell neuroprotection in glaucoma. *Gene Ther*. 2012;19:127–136.
9. Krishnan A, Fei F, Jones A, et al. Overexpression of soluble Fas ligand following adeno-associated virus gene therapy prevents retinal ganglion cell death in chronic and acute murine models of glaucoma. *J Immunol*. 2016;197:4626–4638.
10. Sun D, Moore S, Jakobs TC. Optic nerve astrocyte reactivity protects function in experimental glaucoma and other nerve injuries. *J Exp Med*. 2017;214:1411–1430.
11. Baltan S, Inman DM, Danilov CA, Morrison RS, Calkins DJ, Horner PJ. Metabolic vulnerability disposes retinal ganglion cell axons to dysfunction in a model of glaucomatous degeneration. *J Neurosci*. 2010;30:5644–5652.
12. Cooper ML, Crish SD, Inman DM, Horner PJ, Calkins DJ. Early astrocyte redistribution in the optic nerve precedes axonopathy in the DBA/2J mouse model of glaucoma. *Exp Eye Res*. 2016;150:22–33.
13. Coughlin L, Morrison RS, Horner PJ, Inman DM. Mitochondrial morphology differences and mitophagy deficit in murine glaucomatous optic nerve. *Invest Ophthalmol Vis Sci*. 2015;56:1437–1446.
14. Williams PA, Harder JM, Foxworth NE, et al. Vitamin B3 modulates mitochondrial vulnerability and prevents glaucoma in aged mice. *Science*. 2017;355:756–760.
15. Jiang X, Johnson E, Cepurna W, et al. The effect of age on the response of retinal capillary filling to changes in intraocular pressure measured by optical coherence tomography angiography. *Microvasc Res*. 2018;115:12–19.
16. Hernandez MR, Luo XX, Andrzejewska W, Neufeld AH. Age-related changes in the extracellular matrix of the human optic nerve head. *Am J Ophthalmol*. 1989;107:476–484.

17. Albon J, Purslow PP, Karwatowski WS, Easty DL. Age related compliance of the lamina cribrosa in human eyes. *Br J Ophthalmol*. 2000;84:318–323.
18. Girard MJ, Suh JK, Bottlang M, Burgoyne CF, Downs JC. Scleral biomechanics in the aging monkey eye. *Invest Ophthalmol Vis Sci*. 2009;50:5226–5237.
19. Coudrillier B, Pijanka J, Jefferys J, et al. Effects of age and diabetes on scleral stiffness. *J Biomech Eng*. 2015;137: 071007.
20. Jakobs TC, Libby RT, Ben Y, John SW, Masland RH. Retinal ganglion cell degeneration is topological but not cell type specific in DBA/2J mice. *J Cell Biol*. 2005;171:313–325.
21. Balaratnasingam C, Morgan WH, Bass L, Matich G, Cringle SJ, Yu DY. Axonal transport and cytoskeletal changes in the laminar regions after elevated intraocular pressure. *Invest Ophthalmol Vis Sci*. 2007;48:3632–3644.
22. Howell GR, Libby RT, Jakobs TC, et al. Axons of retinal ganglion cells are insulted in the optic nerve early in DBA/2J glaucoma. *J Cell Biol*. 2007;179:1523–1537.
23. Morcos Y, Chan-Ling T. Concentration of astrocytic filaments at the retinal optic nerve junction is coincident with the absence of intra-retinal myelination: comparative and developmental evidence. *J Neurocytol*. 2000;29:665–678.
24. Sun D, Lye-Barthel M, Masland RH, Jakobs TC. The morphology and spatial arrangement of astrocytes in the optic nerve head of the mouse. *J Comp Neurol*. 2009;516:1–19.
25. Radius RL, Gonzales M. Anatomy of the lamina cribrosa in human eyes. *Arch Ophthalmol*. 1981;99:2159–2162.
26. Lockwood H, Reynaud J, Gardiner S, et al. Lamina cribrosa microarchitecture in normal monkey eyes part 1: methods and initial results. *Invest Ophthalmol Vis Sci*. 2015;56:1618–1637.
27. Morrison J, Farrell S, Johnson E, Deppmeier L, Moore CG, Grossmann E. Structure and composition of the rodent lamina cribrosa. *Exp Eye Res*. 1995;60:127–135.
28. May CA, Lutjen-Drecoll E. Morphology of the murine optic nerve. *Invest Ophthalmol Vis Sci*. 2002;43:2206–2212.
29. Dai C, Khaw PT, Yin ZQ, Li D, Raisman G, Li Y. Structural basis of glaucoma: the fortified astrocytes of the optic nerve head are the target of raised intraocular pressure. *Glia*. 2012;60: 13–28.
30. Sofroniew MV, Vinters HV. Astrocytes: biology and pathology. *Acta Neuropathol*. 2010;119:7–35.
31. Sun D, Jakobs TC. Structural remodeling of astrocytes in the injured CNS. *Neuroscientist*. 2012;18:567–588.
32. Kaja S, Payne AJ, Patel KR, Naumchuk Y, Koulen P. Differential subcellular Ca2+ signaling in a highly specialized subpopulation of astrocytes. *Exp Neurol*. 2015;265:59–68.
33. Mathieu E, Gupta N, Ahari A, Zhou X, Hanna J, Yucel YH. Evidence for cerebrospinal fluid entry into the optic nerve via a glymphatic pathway. *Invest Ophthalmol Vis Sci*. 2017;58: 4784–4791.
34. Ho KW, Lambert WS, Calkins DJ. Activation of the TRPV1 cation channel contributes to stress-induced astrocyte migration. *Glia*. 2014;62:1435–1451.
35. Choi HJ, Sun D, Jakobs TC. Astrocytes in the optic nerve head express putative mechanosensitive channels. *Mol Vis*. 2015; 21:749–766.
36. Nguyen JV, Soto I, Kim KY, et al. Myelination transition zone astrocytes are constitutively phagocytic and have synuclein dependent reactivity in glaucoma. *Proc Natl Acad Sci U S A*. 2011;108:1176–1181.
37. Mills EA, Davis CH, Bushong EA, et al. Astrocytes phagocytose focal dystrophies from shortening myelin segments in the optic nerve of Xenopus laevis at metamorphosis. *Proc Natl Acad Sci U S A*. 2015;112:10509–10514.
38. Davis CH, Kim KY, Bushong EA, et al. Transcellular degradation of axonal mitochondria. *Proc Natl Acad Sci U S A*. 2014;111:9633–9638.
39. Sappington RM, Carlson BJ, Crish SD, Calkins DJ. The microbead occlusion model: a paradigm for induced ocular hypertension in rats and mice. *Invest Ophthalmol Vis Sci*. 2010;51:207–216.
40. Chen H, Wei X, Cho KS, et al. Optic neuropathy due to microbead-induced elevated intraocular pressure in the mouse. *Invest Ophthalmol Vis Sci*. 2011;52:36–44.
41. Wang R, Seifert P, Jakobs TC. Astrocytes in the optic nerve head of glaucomatous mice display a characteristic reactive phenotype. *Invest Ophthalmol Vis Sci*. 2017;58:924–932.
42. Zarei K, Scheetz TE, Christopher M, et al. Automated axon counting in rodent optic nerve sections with AxonJ. *Sci Rep*. 2016;6:26559.
43. Li Y, Li D, Ying X, Khaw PT, Raisman G. An energy theory of glaucoma. *Glia*. 2015;63:1537–1552.
44. Morrison JC, Cepurna WO, Tehrani S, et al. A period of controlled elevation of IOP (CEI) produces the specific gene expression responses and focal injury pattern of experimental rat glaucoma. *Invest Ophthalmol Vis Sci*. 2016;57:6700–6711.
45. Dutta S, Sengupta P. Men and mice: relating their ages. *Life Sci*. 2016;152:244–248.
46. Flurkey K, Currer JM, Harrison DE. Mouse models in aging research. In: Fox JG, Davisson MT, Quimby FW, Barthold SW, Newcomer CE, Smith AL, eds. *The Mouse in Biomedical Research*. Burlington, MA: Elsevier; 2007:637–672.
47. Tham YC, Li X, Wong TY, Quigley HA, Aung T, Cheng CY. Global prevalence of glaucoma and projections of glaucoma burden through 2040: a systematic review and meta-analysis. *Ophthalmology*. 2014;121:2081–2090.
48. Calkins DJ. Age-related changes in the visual pathways: blame it on the axon. *Invest Ophthalmol Vis Sci*. 2013;54:ORSF37–ORSF41.
49. Repka MX, Quigley HA. The effect of age on normal human optic nerve fiber number and diameter. *Ophthalmology*. 1989;96:26–32.
50. Cepurna WO, Kayton RJ, Johnson EC, Morrison JC. Age related optic nerve axonal loss in adult Brown Norway rats. *Exp Eye Res*. 2005;80:877–884.
51. Feng L, Sun Z, Han H, Zhou Y, Zhang M. No age-related cell loss in three retinal nuclear layers of the Long-Evans rat. *Vis Neurosci*. 2007;24:799–803.
52. Mikelberg FS, Drance SM, Schulzer M, Yidegiligne HM, Weis MM. The normal human optic nerve. Axon count and axon diameter distribution. *Ophthalmology*. 1989;96:1325–1328.
53. Morrison JC, Cork LC, Dunkelberger GR, Brown A, Quigley HA. Aging changes of the rhesus monkey optic nerve. *Invest Ophthalmol Vis Sci*. 1990;31:1623–1627.
54. Jonas JB, Schmidt AM, Müller-Bergh JA, Schlotzer-Schrehardt UM, Naumann GO. Human optic nerve fiber count and optic disc size. *Invest Ophthalmol Vis Sci*. 1992;33:2012–2018.
55. Danias J, Lee KC, Zamora MF, et al. Quantitative analysis of retinal ganglion cell (RGC) loss in aging DBA/2NNia glaucomatous mice: comparison with RGC loss in aging C57/BL6 mice. *Invest Ophthalmol Vis Sci*. 2003;44:5151–5162.
56. Esquiva G, Lax P, Perez-Santonja JJ, Garcia-Fernandez JM, Cuenca N. Loss of melanopsin-expressing ganglion cell subtypes and dendritic degeneration in the aging human retina. *Front Aging Neurosci*. 2017;9:79.
57. Neufeld AH, Gachie EN. The inherent, age-dependent loss of retinal ganglion cells is related to the lifespan of the species. *Neurobiol Aging*. 2003;24:167–172.

58. Wang L, Dong J, Cull G, Fortune B, Cioffi GA. Varicosities of intraretinal ganglion cell axons in human and nonhuman primates. *Invest Ophthalmol Vis Sci*. 2003;44:2–9.
59. Quigley HA, Addicks EM. Chronic experimental glaucoma in primates. II. Effect of extended intraocular pressure elevation on optic nerve head and axonal transport. *Invest Ophthalmol Vis Sci*. 1980;19:137–152.
60. Johansson JO. Inhibition of retrograde axoplasmic transport in rat optic nerve by increased IOP in vitro. *Invest Ophthalmol Vis Sci*. 1983;24:1552–1558.
61. Quigley HA, McKinnon SJ, Zack DJ, et al. Retrograde axonal transport of BDNF in retinal ganglion cells is blocked by acute IOP elevation in rats. *Invest Ophthalmol Vis Sci*. 2000;41:3460–3466.
62. Crish SD, Dapper JD, MacNamee SE, et al. Failure of axonal transport induces a spatially coincident increase in astrocyte BDNF prior to synapse loss in a central target. *Neuroscience*. 2013;229:55–70.
63. Hollenbeck PJ, Saxton WM. The axonal transport of mitochondria. *J Cell Sci*. 2005;118:5411–5419.
64. Chrysostomou V, Rezania F, Trounce IA, Crowston JG. Oxidative stress and mitochondrial dysfunction in glaucoma. *Curr Opin Pharmacol*. 2013;13:12–15.
65. Stahon KE, Bastian C, Griffith S, Kidd GJ, Brunet S, Baltan S. Age-related changes in axonal and mitochondrial ultrastructure and function in white matter. *J Neurosci*. 2016;36:9990–10001.
66. Kamel K, Farrell M, O'Brien C. Mitochondrial dysfunction in ocular disease: focus on glaucoma. *Mitochondrion*. 2017;35:44–53.
67. Lascaratos G, Chau KY, Zhu H, et al. Resistance to the most common optic neuropathy is associated with systemic mitochondrial efficiency. *Neurobiol Dis*. 2015;82:78–85.
68. Lee S, Van Bergen NJ, Kong GY, et al. Mitochondrial dysfunction in glaucoma and emerging bioenergetic therapies. *Exp Eye Res*. 2011;93:204–212.
69. Gueven N, Nadikudi M, Daniel A, Chhetri J. Targeting mitochondrial function to treat optic neuropathy. *Mitochondrion*. 2017;36:7–14.
70. Ju WK, Kim KY, Lindsey JD, et al. Intraocular pressure elevation induces mitochondrial fission and triggers OPA1 release in glaucomatous optic nerve. *Invest Ophthalmol Vis Sci*. 2008;49:4903–4911.
71. Kim KY, Perkins GA, Shim MS, et al. DRP1 inhibition rescues retinal ganglion cells and their axons by preserving mitochondrial integrity in a mouse model of glaucoma. *Cell Death Dis*. 2015;6:e1839.
72. Ju WK, Kim KY, Noh YH, et al. Increased mitochondrial fission and volume density by blocking glutamate excitotoxicity protect glaucomatous optic nerve head astrocytes. *Glia*. 2015;63:736–753.
73. Harris JJ, Attwell D. The energetics of CNS white matter. *J Neurosci*. 2012;32:356–371.
74. Hernandez MR, Ye H, Roy S. Collagen type IV gene expression in human optic nerve heads with primary open angle glaucoma. *Exp Eye Res*. 1994;59:41–51.
75. Gottanka J, Kuhlmann A, Scholz M, Johnson DH, Lutjen-Drecoll E. Pathophysiologic changes in the optic nerves of eyes with primary open angle and pseudoexfoliation glaucoma. *Invest Ophthalmol Vis Sci*. 2005;46:4170–4181.
76. Sun D, Qu J, Jakobs TC. Reversible reactivity by optic nerve astrocytes. *Glia*. 2013;61:1218–1235.
77. Tehrani S, Johnson EC, Cepurna WO, Morrison JC. Astrocyte processes label for filamentous actin and reorient early within the optic nerve head in a rat glaucoma model. *Invest Ophthalmol Vis Sci*. 2014;55:6945–6952.
78. Tehrani S, Davis L, Cepurna WO, et al. Astrocyte structural and molecular response to elevated intraocular pressure occurs rapidly and precedes axonal tubulin rearrangement within the optic nerve head in a rat model. *PLoS One*. 2016;11:e0167364.
79. Hernandez MR, Miao H, Lukas T. Astrocytes in glaucomatous optic neuropathy. *Prog Brain Res*. 2008;173:353–373.
80. Schlamp CL, Li Y, Dietz JA, Janssen KT, Nickells RW. Progressive ganglion cell loss and optic nerve degeneration in DBA/2J mice is variable and asymmetric. *BMC Neurosci*. 2006;7:66.